

Glitoxin Suppresses Macrophage Immune Function by Subverting Phosphatidylinositol 3,4,5-Trisphosphate Homeostasis

Daniel Schlam,^{a,b} Johnathan Canton,^a Marvin Carreño,^a Hannah Kopinski,^{a*} Spencer A. Freeman,^a Sergio Grinstein,^{a,b,c} Gregory D. Fairn^{b,c,d}

Division of Cell Biology, Hospital for Sick Children, Toronto, Ontario, Canada^a; Faculty of Medicine, Institute of Medical Science, University of Toronto, Toronto, Ontario, Canada^b; Keenan Research Centre for Biomedical Science, St. Michael's Hospital, Toronto, Ontario, Canada^c; Departments of Surgery and Biochemistry, University of Toronto, Toronto, Ontario, Canada^d

* Present address: Hannah Kopinski, New York University School of Medicine, New York, New York, USA.

ABSTRACT *Aspergillus fumigatus*, an opportunistic fungal pathogen, spreads in the environment by releasing numerous conidia that are capable of reaching the small alveolar airways of mammalian hosts. In otherwise healthy individuals, macrophages are responsible for rapidly phagocytosing and eliminating these conidia, effectively curbing their germination and consequent invasion of pulmonary tissue. However, under some circumstances, the fungus evades phagocyte-mediated immunity and persists in the respiratory tree. Here, we report that *A. fumigatus* escapes macrophage recognition by strategically targeting phosphatidylinositol 3,4,5-trisphosphate [PtdIns(3,4,5)P₃] metabolism through gliotoxin, a potent immunosuppressive mycotoxin. Time-lapse microscopy revealed that, in response to the toxin, macrophages cease to ruffle, undergo abrupt membrane retraction, and fail to phagocytose large targets effectively. Gliotoxin was found to prevent integrin activation and interfere with actin dynamics, both of which are instrumental for phagocytosis; similar effects were noted in immortalized and primary phagocytes. Detailed studies of the underlying molecular mechanisms of toxicity revealed that inhibition of phagocytosis is attributable to impaired accumulation of PtdIns(3,4,5)P₃ and the associated dysregulation of downstream effectors, including Rac and/or Cdc42. Strikingly, in response to the diacylglycerol mimetic phorbol 12-myristate 13-acetate, gliotoxin-treated macrophages reactivate beta integrins, reestablish actin dynamics, and regain phagocytic capacity, despite the overt absence of plasma-memmal PtdIns(3,4,5)P₃. Together, our findings identify phosphoinositide metabolism as a critical upstream target of gliotoxin and also indicate that increased diacylglycerol levels can bypass the requirement for PtdIns(3,4,5)P₃ signaling during membrane ruffling and phagocytosis.

IMPORTANCE *Aspergillus fumigatus* is the most frequent cause of human infections in the *Aspergillus* genus. In immunocompromised populations, invasive aspergillosis (IA) is associated with a mortality rate of up to 90%, and current antifungal therapies have failed to prevent or reverse the infection. Therefore, a deeper understanding of the interactions between *A. fumigatus* and its host is required. In healthy humans, alveolar macrophages can ingest and eliminate fungal spores, thus limiting their germination into mycotoxin-producing hyphae. Our studies reveal that gliotoxin—the most abundant *Aspergillus* mycotoxin—undermines the ability of phagocytes to carry out their protective functions. By targeting PtdIns(3,4,5)P₃ signaling and down-regulating phagocytic immune defenses, the toxin could also exacerbate polymicrobial infections. Notably, we were able to reverse gliotoxin toxicity by addition of diacylglycerol analogues, which may provide the basis for therapeutic interventions.

Received 26 December 2015 Accepted 6 March 2016 Published 5 April 2016

Citation Schlam D, Canton J, Carreño M, Kopinski H, Freeman SA, Grinstein S, Fairn GD. 2016. Gliotoxin suppresses macrophage immune function by subverting phosphatidylinositol 3,4,5-trisphosphate homeostasis. *mBio* 7(2):e02242-15. doi:10.1128/mBio.02242-15.

Editor Michele S. Swanson, University of Michigan

Copyright © 2016 Schlam et al. This is an open-access article distributed under the terms of the [Creative Commons Attribution-Noncommercial-ShareAlike 3.0 Unported license](https://creativecommons.org/licenses/by-nc-sa/4.0/), which permits unrestricted noncommercial use, distribution, and reproduction in any medium, provided the original author and source are credited.

Address correspondence to Gregory D. Fairn, fairng@smh.ca.

The opportunistic mold *Aspergillus fumigatus* is the primary causative agent of invasive aspergillosis (IA), a devastating disease with a mortality rate of almost 90% in high-risk populations (1). While immunosuppressed individuals—including patients receiving a bone marrow transplant or undergoing chemotherapy—are most susceptible to *A. fumigatus* infections (2), this pathogen is also frequently isolated from sputum samples from patients with chronic respiratory diseases, such as cystic fibrosis (3, 4).

Similar to other saprophytic fungi, *A. fumigatus* is virtually

omnipresent in the environment as a natural occupant of soil and plants (5). It spreads by releasing copious quantities of airborne conidia, nonmotile dormant spores that can infiltrate the small alveolar airways upon inhalation. As a necessary complement to the mucociliary apparatus, lung-resident (alveolar) macrophages recognize, internalize, and rapidly dispose of the hundreds of *Aspergillus* conidia that the average person inhales every day (6, 7), thereby preventing their germination and the formation of pulmonary hyphal networks (8–10). Of note, the establishment of hyphal networks by *A. fumigatus* is accompanied by the secretion

of several immunosuppressive mycotoxins (11). The most abundant of these mycotoxins is gliotoxin (12), a secondary metabolite with a wide range of immunomodulating capabilities (13–18) and associated with the development of IA (11). Like other toxins of the epipolythiodioxopiperazine class, gliotoxin carries an internal disulfide bridge that is essential for virulence (19).

Given that *Aspergillus* conidia are metabolically inactive, it is only the hyphal morphotype that is capable of synthesizing and secreting toxic secondary metabolites, including gliotoxin. Under otherwise physiological conditions, alveolar macrophages rapidly phagocytose inhaled conidia in order to prevent the formation of these hyphal networks. However, in individuals with impaired mucociliary clearance or suffering from immunodeficiencies, alveolar macrophages cannot effectively contend with the increased and consistent burden of *Aspergillus* spores. The latter markedly increases the susceptibility to mycelial colonization and to the consequent destruction of pulmonary tissue. Thus, while alveolar macrophages are normally instrumental in preventing hyphal colonization of the lung, underlying susceptibilities to infection (such as immunosuppression or respiratory conditions) may overwhelm phagocytic defenses and permit conidial germination. Gliotoxin secretion by newly established hyphae may then further suppress phagocytic defenses, thus intensifying an infection and inflammation cycle.

Here, we test the notion that gliotoxin exacerbates microbial infection by impairing the mechanisms employed by macrophages for recognizing, taking up, and destroying invading pathogens. We find that gliotoxin markedly interferes with PtdIns(3,4,5)P₃ production, thereby precluding the extension of actin-driven membrane protrusions utilized by macrophages to survey their environment. PtdIns(3,4,5)P₃ dysregulation results in overt integrin and actin cytoskeletal defects, profoundly affecting the ability of macrophages to remain adherent to the substratum and to complete phagocytosis of relatively large targets. Interestingly, these abnormalities can be reversed by the addition of a diacylglycerol analogue to gliotoxin-treated cells. Overall, our observations identify PtdIns(3,4,5)P₃ as a novel and critical gliotoxin target in phagocytes and suggest that PtdIns(3,4,5)P₃-mediated diacylglycerol biosynthesis is key to the extensive actin remodeling and integrin response required for cell spreading and phagocytosis.

RESULTS

Gliotoxin inhibits diverse phagocytic modalities in macrophages. To characterize the effect of the toxin on phagocytosis, we incubated murine RAW 264.7 macrophages with gliotoxin (500 ng/ml; 1.53 μ M) or vehicle (dimethyl sulfoxide [DMSO]) for 30 min. Immediately thereafter, IgG-opsonized red blood cells (IgG-RBC) that had been prelabeled with a Cy3-conjugated secondary antibody were sedimented onto the macrophages to initiate Fc γ receptor (Fc γ R)-mediated phagocytosis, which was allowed to proceed for 10 min before washing and fixing. IgG-RBC that remained adherent to the cell surface but were not internalized were identified by incubating the fixed, nonpermeabilized cells with Cy5-conjugated anti-IgG. Thus, our phagocytic assay distinguished noninternalized targets (both Cy5 and Cy3 positive) from internalized targets (Cy3 positive only). Macrophages were subsequently permeabilized with Triton X-100 and stained with Alexa Fluor 488-conjugated phalloidin to visualize actin fila-

ments. As shown in Fig. 1A and B, gliotoxin-treated macrophages exhibited a steep decline in phagocytic ability compared to untreated controls; not only did the toxin preclude binding to phagocytic targets, it also hindered their subsequent internalization. As quantified in Fig. 1G, the inhibitory effect of gliotoxin on Fc γ R-mediated phagocytosis was dose dependent. The gliotoxin doses employed in this assay, from 62.5 to 1,000 ng/ml, are in the range of concentrations detected in serum samples of patients with invasive aspergillosis (IA), which varies between \approx 150 and 800 ng/ml (20). Gliotoxin must be present at even higher concentrations in the lung parenchyma, the primary location of invasive hyphal growth. Indeed, analyses of mice with experimentally induced IA have shown that gliotoxin is typically found in the lung at approximately 4,000 ng/g of tissue (20).

The fact that gliotoxin subverted phagocytosis of IgG-coated particles in RAW 264.7 cells prompted us to investigate whether the toxin had comparable effects on the engulfment of fungal particles by primary macrophages. To this end, we used either serum-coated or unopsonized zymosan as phagocytic targets for human monocyte-derived macrophages (Fig. 1C to F). Zymosan is ideally suited for the study of phagocytosis of fungal particles, as it is prepared from yeast cell walls and carries on its surface β (1,3)-glucans that are recognized by the phagocytic receptor dectin-1. To facilitate their visualization by microscopy, we simultaneously labeled all zymosan particles with succinimidyl esters conjugated to either Alexa Fluor 555 (shown in red in Fig. 1C to F) or to biotin. These functionalized zymosan particles were then sedimented onto macrophages to initiate phagocytosis, which was allowed to proceed for 20 min before fixation. Noninternalized particles were identified by labeling the biotin tag with fluorescent streptavidin (shown in blue). Similar to the effects observed for Fc γ R-mediated phagocytosis, gliotoxin profoundly depressed both binding and engulfment of serum-coated zymosan (Fig. 1C and D), which is normally engulfed upon engagement of both Fc γ R and complement receptors. Likewise, dectin-1-mediated phagocytosis of unopsonized zymosan (Fig. 1E and F) by human macrophages was virtually obliterated by gliotoxin. As quantified in Fig. 1H, the total number of serum-opsonized zymosan particles engaged by macrophages (white bars) decreased from 9.4 ± 1.3 to 3.1 ± 0.7 upon gliotoxin treatment. This effect was even more striking for unopsonized zymosan; the total number of contacted particles was reduced from 4.4 ± 0.6 to 0.22 ± 0.08 . Thus, for both serum-opsonized and unopsonized zymosan, gliotoxin exposure led to a more than 4-fold drop in phagocytic efficiency (the ratio of internalized to total number of engaged particles; shown as a percentage above the bars in Fig. 1H).

Macrophage viability is not compromised after acute gliotoxin exposure. Prolonged exposure to gliotoxin has been reported to trigger apoptosis (12, 15, 21). While our gliotoxin treatments were comparably short (15 to 30 min), we nevertheless questioned whether the gliotoxin-mediated phagocytic impairment we observed was attributable to reduced macrophage viability. We addressed this by two independent, complementary assays (see Fig. S1 in the supplemental material). First, we monitored plasmalemmal integrity in gliotoxin-treated RAW 264.7 macrophages using the membrane-impermeant dye aqua LIVE/DEAD. This fluorescent molecule exclusively stains plasmalemmal proteins of live cells, but it gains access to the cytoplasm of necrotic cells because of their increased membrane permeability. As illustrated in Fig. S1A and S1B, the vast majority ($93.2\% \pm 1.7\%$) of

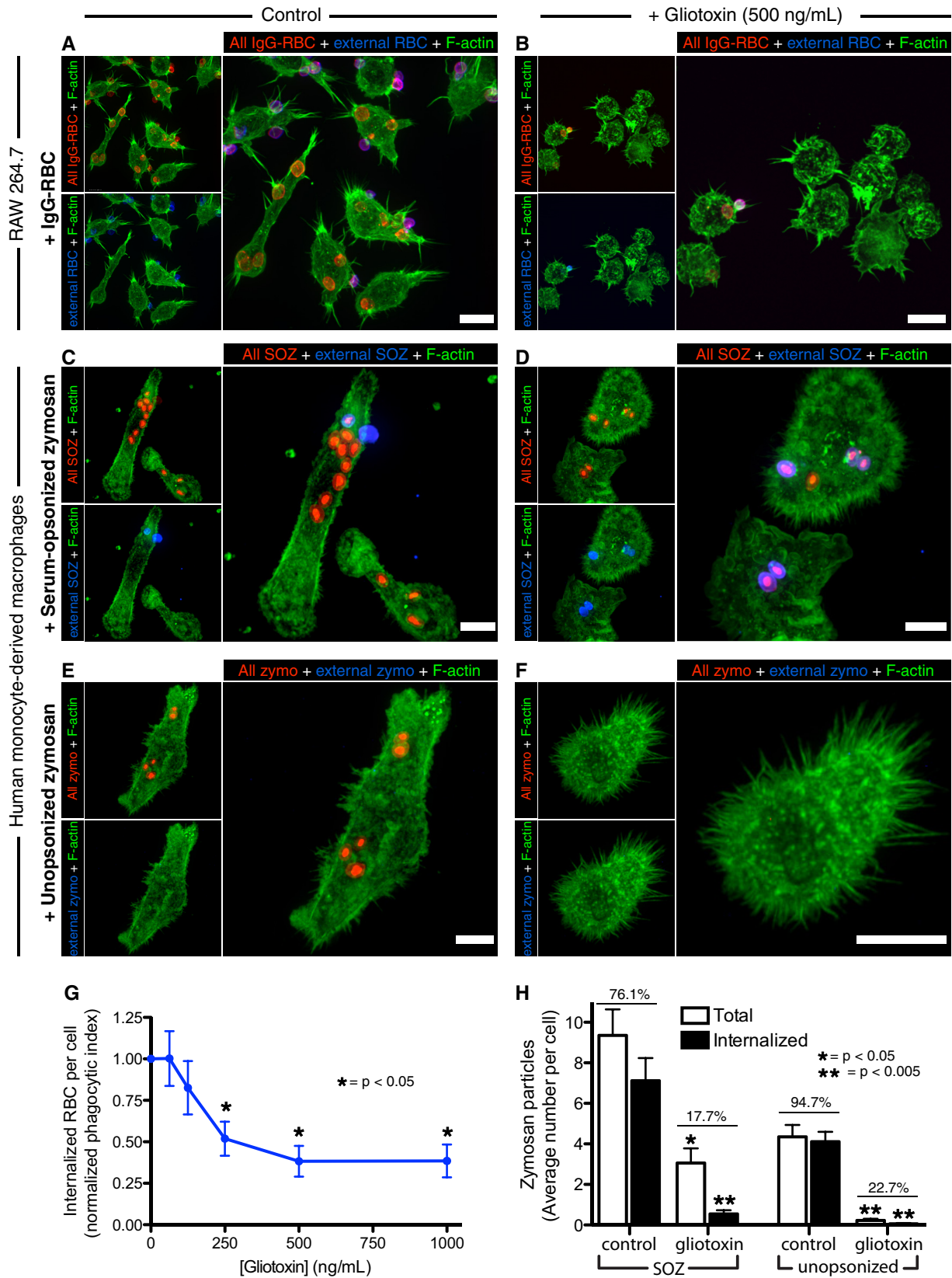


FIG 1 Gliotoxin inhibits phagocytosis in macrophages. (A to F) RAW 264.7 cells (A and B) and human monocyte-derived macrophages (C to F) were treated with vehicle only (DMSO) (left panels) or 500 ng/ml gliotoxin (right panels) for 30 min immediately before being challenged with IgG-opsonized red blood cells (A and B), serum-opsonized zymosan (C and D), or unopsonized zymosan (E and F). In all instances, phagocytosis proceeded for 20 min before fixation. All IgG-coated erythrocytes were labeled with Cy3-conjugated IgG (shown in red) prior to the onset of phagocytosis. To identify erythrocytes that were not

(Continued)

gliotoxin-treated macrophages maintained plasmalemmal integrity even 4 h after gliotoxin exposure (as evident by the absence of cytoplasmic fluorescence), implying that these cells were not undergoing necrosis. Second, to assess whether short gliotoxin incubations resulted in apoptosis, we monitored phosphatidylserine (PtdSer) exposure on the exofacial leaflet of the plasma membrane and also nuclear condensation, using annexin V and 4',6'-diamidino-2-phenylindole (DAPI) staining, respectively. As shown in Fig. S1C and S1D, PtdSer asymmetry was maintained for the first 2 h of treatment, with $87.8\% \pm 4\%$ of the cells remaining annexin V negative and therefore not apoptotic at this time. Of note, no indications of cell death were observed for periods of time greatly exceeding the one used for our phagocytic assays. Indeed, the gliotoxin-induced phagocytic and cytoskeletal abnormalities shown in Fig. 1 were fully apparent within 15 min of gliotoxin treatment. Thus, a mechanism other than cell death must account for the acute phagocytic impairment elicited by gliotoxin.

Cell-surface distribution and affinity of FcγR are not altered by gliotoxin. The marked reduction in the ability of gliotoxin-treated macrophages to engage their targets may have been caused by a reduction in the number of phagocytic receptors at the cell surface and/or of their ability to recognize their ligand. We examined these possibilities by a combination of immunofluorescence and flow cytometry. Figure 2A to D show representative micrographs of control (left panels) and gliotoxin-treated (right panels) RAW 264.7 cells that were stained with antibodies against Fcγ receptor I (FcγRI) (Fig. 2A and B) or against an epitope shared by FcγRIIb and FcγRIII (Fig. 2C and D). As evident in these images, the levels of cell-surface Fcγ receptors were comparable in DMSO- and gliotoxin-treated cells. The density of FcγRI and FcγRIIb/FcγRIII at the cell surface was also quantified by flow cytometry (Fig. 2G and H), which confirmed that the distribution of these receptors did not change upon gliotoxin treatment.

To assess whether gliotoxin reduced receptor affinity, we next compared the ability of control and gliotoxin-treated macrophages to bind fluorescent IgG aggregates (Fig. 2E and F). These assays, performed at 16°C to avoid internalization of the aggregates, revealed no significant differences between DMSO- and gliotoxin-treated macrophages (Fig. 2I). Together, these data indicate that neither a change in the number of receptors nor in their affinity for IgG can account for the impairment of phagocytosis by gliotoxin.

Cell adhesion and actin dynamics are profoundly affected by gliotoxin. To aid us in identifying likely targets of the toxin in phagocytes, we compared the ultrastructure of human monocyte-derived macrophages under control and gliotoxin treatment conditions, using scanning electron microscopy. As the representative micrographs in Fig. 3 show, gliotoxin treatment prevented the elaboration of lamellipodial extensions, which were otherwise prominent under control conditions (Fig. 3A). Instead, macro-

phages exposed to the toxin lost adhesion to the substratum, forming retraction fibers (Fig. 3B). The capacity of gliotoxin to dually interfere with actin dynamics and cell adhesion was also observed by time-lapse differential interference contrast (DIC) microscopy; Movie S1 in the supplemental material shows that RAW 264.7 cells withdrew their actin-driven membrane extensions and abruptly retracted in response to the mycotoxin. Likewise, the phagocytic response and highly dynamic membrane protrusions of primary human macrophages (Movie S2) were virtually obliterated upon gliotoxin treatment (Movie S3).

The scanning electron microscopy examination also revealed that gliotoxin-treated macrophages responded to serum-opsonized zymosan by developing abortive phagocytic cups, which arrested halfway around the particle (Fig. 3D, inset). Previous studies have shown that macrophages incubated with phosphatidylinositol 3-kinase (PI3K) inhibitors such as LY294002 or wortmannin arrest at similar stages of phagocytosis (22–24), generating unproductive cups or membrane pedestals akin to those shown in Fig. 3D.

Given its striking effect on the ability of macrophages to extend and maintain actin-driven protrusions, we next questioned whether the cellular level of filamentous actin (F-actin) was altered by gliotoxin. RAW 264.7 macrophages were treated with increasing concentrations of the toxin for 30 min immediately before being fixed, permeabilized, and stained with fluorescent phalloidin (Fig. 3E and F). Cells were then imaged by confocal microscopy, and the intensity of phalloidin fluorescence was used as an indicator of the F-actin level. As shown in Fig. 3F, gliotoxin treatment led to a dose-dependent decline in the F-actin content of the cells.

Gliotoxin-induced cytoskeletal abnormalities are accompanied by Rac/Cdc42 inactivation. The small Rho GTPases Rac and Cdc42 orchestrate the initial projection and progression of actin-driven pseudopodia around phagocytic targets (25–29). Rac is also responsible for driving the constitutive membrane ruffling of professional phagocytes (30). We therefore tested the effects of gliotoxin on these GTPases. To this end, we cotransfected macrophages with constructs encoding PAK(PBD)-YFP, the p21-binding domain (PBD) of p21-activated kinase (PAK) conjugated to yellow fluorescent protein (YFP), and Lifeact-mRFP (mRFP stands for monomeric red fluorescent protein), fluorescent biosensors of active (GTP-loaded) Rac/Cdc42 (27, 31) and F-actin (31), respectively. Transfectants were imaged live by time-lapse confocal microscopy under control conditions and immediately after gliotoxin exposure (see Movie S4 for uninterrupted time-lapse sequence). As expected, control macrophages constitutively generated actin-rich membrane ruffles (Fig. 3G, top panel), and these disappeared upon gliotoxin addition (Fig. 3H, top panel). More importantly, retraction of these membrane projections was coincident in space and time with the dissociation of PAK(PBD)-

Figure Legend Continued

internalized, the fixed cells were stained with a Cy5-conjugated antibody (shown in blue) following phagocytosis. Likewise, all zymosan particles were simultaneously labeled with succinimidyl esters of Alexa Fluor 555 (shown in red) or of biotin prior to initiating phagocytosis. Bound but nonphagocytosed zymosan was visualized by staining with streptavidin-Alexa Fluor 647 (shown in blue). Macrophages were then permeabilized and stained with phalloidin-Alexa Fluor 488 to visualize F-actin. All images are displayed as Z-projections of confocal sections. Bars = 10 μm. (G) Quantification of the average number of IgG-opsonized erythrocytes internalized per RAW 264.7 cell in response to the indicated gliotoxin concentrations. (H) Quantification of the total (white bars) and internalized (black bars) number of serum-opsonized or unopsonized zymosan particles associated per human macrophage. The ratio of internalized-to-total number of particles is indicated as a percentage above the bars. All experiments were conducted independently at least three times, and error bars represent the standard errors of the means (SEM). IgG-RBC, IgG-opsonized red blood cells; SOZ, serum-opsonized zymosan.

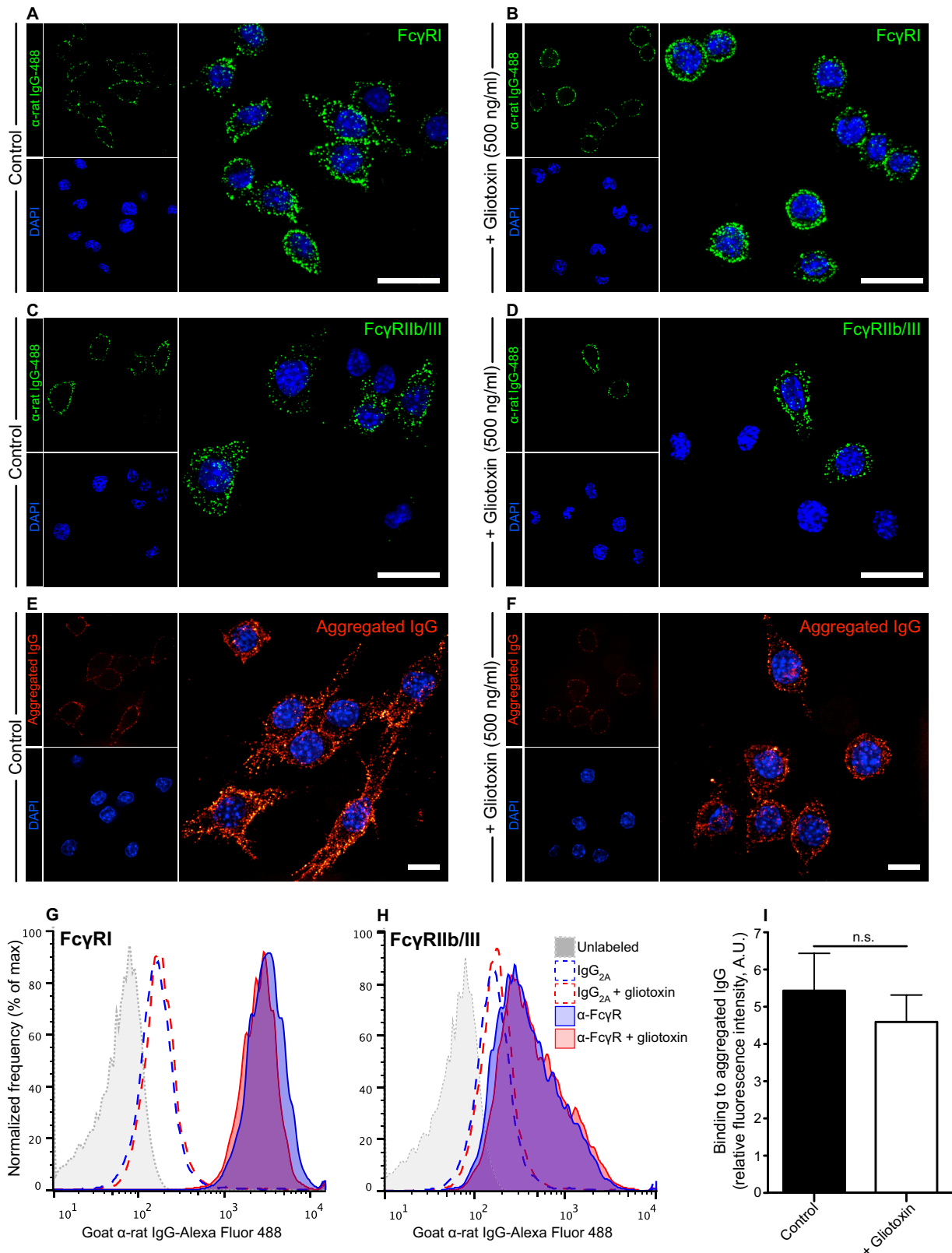


FIG 2 Surface density and binding ability of Fc γ receptors are unaltered by gliotoxin. (A to F) RAW 2.7 cells were treated with vehicle alone (DMSO) (left panels) or 500 ng/ml gliotoxin (right panels) for 30 min immediately before being labeled with either anti-Fc γ RI (α -Fc γ RI) (A and B) or anti-Fc γ RIIb/III (C and D) antibodies or exposed to Cy3-conjugated aggregated IgG (E and F). Surface expression of the indicated Fc γ receptors (shown in green) was visualized by staining with Alexa Fluor 488-conjugated secondary antibodies, while nuclei were counterstained with DAPI (shown in blue). For each individual panel in panels A to F, channels are shown either individually as confocal XY sections (smaller images, left side), or merged as a Z-projection (larger image, right side). Bars = 10 μ m.

(Continued)

YFP from sites of actin polymerization (Fig. 3G and H, bottom panels), suggesting that gliotoxin interferes with homeostatic actin dynamics by precluding activation of Rac and/or Cdc42.

Treatment with gliotoxin does not trigger cAMP signaling in macrophages. A previous study reported that gliotoxin induces marked alterations in the actin cytoskeleton of neutrophils (32). The authors noted that stimulation of cyclic AMP (cAMP) signaling in neutrophils recapitulated (some of) the gliotoxin-induced cytoskeletal abnormalities. Conversely, these actin defects were prevented if gliotoxin treatment was preceded by incubating the neutrophils with (*R*)-adenosine, cyclic 3',5'-(hydrogenphosphorothioate) trimethylammonium (cAMPS-Rp), a competitive inhibitor of cAMP signaling (32). To investigate whether the profound alterations in actin dynamics we observed in macrophages were also cAMP dependent, we conducted two independent assays. First, we assessed the activation state of protein kinase A (PKA), a cAMP-dependent kinase, by monitoring phosphorylation of its substrate, vasodilator-stimulated phosphoprotein (VASP), at serine 157 (33, 34). Surprisingly, the levels of phosphorylated VASP (phospho-VASP) were equivalent in resting and gliotoxin-treated macrophages (see Fig. S3A and S3B in the supplemental material), implying that gliotoxin does not elevate cAMP in macrophages. In contrast, treatment with forskolin—a direct activator of the adenylyl cyclase (35, 36)—led to a more than 80-fold increase in phospho-VASP levels, and this was blunted by incubating the macrophages with cAMPS-Rp prior to forskolin stimulation. Given that our findings were not congruent with gliotoxin toxicity being cAMP dependent, we also assessed cAMP levels by measuring integrin activation; previous work has demonstrated the existence of cAMP-dependent guanine nucleotide exchange factors (GEFs) that promote inside-out activation of integrins through Rap1 (37, 38). Thus, if cAMP levels increased as a consequence of gliotoxin exposure, then integrin activation would ensue. Human monocyte-derived macrophages were treated with gliotoxin or vehicle alone, fixed, and stained with an antibody that recognizes an epitope exposed on activated (high-affinity) integrin β_2 . As a positive control, integrins were activated by incubating with the phorbol ester phorbol myristate acetate (PMA) (Fig. S3C and D). Contrary to the consequences expected from elevation of cAMP, gliotoxin treatment reduced integrin activation (Fig. S3C, top panels; Fig. S3D). Moreover, preincubation of macrophages with gliotoxin significantly precluded PMA-mediated integrin activation (Fig. S3C, bottom panels; Fig. S3D). The failure of gliotoxin to increase VASP phosphorylation, in conjunction with the observed decline in integrin activation, implies that the toxin operates through a mechanism other than triggering cAMP signaling in macrophages.

Gliotoxin decreases PtdIns(3,4,5)P₃ levels in phagocytes. We next turned our attention to phosphoinositides, which play a central role in signaling actin polymerization and remodeling (39). In particular, PtdIns(4,5)P₂ promotes the formation of actin networks and their anchorage to the plasmalemma (40–43), while

PtdIns(3,4,5)P₃ recruits and activates modulators of Rho GTPase activity carrying pleckstrin homology (PH) domains. For instance, the GEFs Vav, Sos1, and Tiam1 induce Rac1 signaling in spatially restricted membrane regions enriched in PtdIns(3,4,5)P₃ (30, 44, 45). To investigate whether gliotoxin-induced alterations in actin dynamics and in Rac/Cdc42 activity were due to a dysregulation in phosphoinositide metabolism, we visualized the cellular distribution of PtdIns(4,5)P₂ and PtdIns(3,4,5)P₃ with the PLC δ (PH)-GFP (PLC stands for phospholipase C, and GFP stands for green fluorescent protein) and Akt(PH)-GFP fluorescent biosensors, respectively (46, 47) (Fig. 4A to E). As expected, PLC δ (PH)-GFP was found along the entire plasmalemma—where PtdIns(4,5)P₂ is most abundant—while Akt(PH)-GFP was largely restricted to membrane ruffles. Remarkably, gliotoxin addition caused dissociation of both biosensors from the plasma membrane (Fig. 4B and D), implying that the concentration of both PtdIns(4,5)P₂ and PtdIns(3,4,5)P₃ decreased. While plasmalemmal PtdIns(4,5)P₂ was only modestly reduced, PtdIns(3,4,5)P₃ was virtually undetectable following gliotoxin treatment (see Fig. 4E for a quantification of normalized fluorescence).

To ensure that the observed decline in PtdIns(3,4,5)P₃ was not an artifact caused by interference of the toxin with the biosensor itself, we also measured Akt phosphorylation at serine 473 by immunoblotting, a commonly used indicator of PtdIns(3,4,5)P₃ abundance (48). As shown in Fig. 4F and G, Akt phosphorylation was markedly reduced in gliotoxin-treated cells compared with controls. Note that cells exposed to gliotoxin exhibited a decline in Akt phosphorylation equivalent to that observed in cells treated with the customary PI3K inhibitor wortmannin (Fig. 4F and G). These observations indicate that gliotoxin interferes with PtdIns(3,4,5)P₃ homeostasis and implicate PI3K as a likely target of the toxin. The data also suggest that the rapid inactivation of Rac/Cdc42 and the ensuing actin cytoskeletal abnormalities may be attributable to a reduction of plasmalemmal PtdIns(3,4,5)P₃.

Gliotoxin-induced inhibition of phagocytosis is dependent on particle size. While similar at first glance, phagocytosis of differently sized particles varies significantly at the molecular level. In particular, phagocytosis of large targets is dependent on PI3K activity, while that of small targets is not (21). Indeed, we and others have shown that cells treated with conventional PI3K inhibitors fail to internalize large (>5- μ m) prey, instead developing actin-rich pseudopodia that arrest halfway around the target (21, 23, 24). Notably, PI3K inhibitors do not similarly affect internalization of smaller targets. This differential requirement of PI3K activity for phagocytosis, in conjunction with our observation that gliotoxin markedly interfered with PtdIns(3,4,5)P₃ levels, led us to hypothesize that internalization of large—and not that of small—targets would be affected by gliotoxin. We tested this notion by challenging gliotoxin-treated macrophages with either large (8.3- μ m) or small (1.6- μ m) IgG-opsonized beads, allowing phagocytosis to proceed for 10 min before fixation. As shown in Fig. S2A in

Figure Legend Continued

α -rat IgG-488, anti-rat IgG conjugated to Alexa Fluor 488. (G and H) Flow cytometry histograms depicting the relative frequency of Fc γ RI-positive (G) and Fc γ RIIb/III-positive (H) RAW 264.7 cells under control (solid blue trace) and gliotoxin (solid red trace) conditions. Isotype traces, indicative of antibody-receptor interactions that occurred through the IgG2a Fc portion (as opposed to the variable region) are shown in dashed lines. The background signal (unlabeled macrophages) is depicted by the gray trace. (I) Quantification of the results shown in panels E and F. Relative fluorescence intensity of Cy3-conjugated aggregated IgG at the cell surface, representative of the affinity of Fc γ receptors for their ligand, is reported for control cells (black bars) and gliotoxin-treated cells (white bars). Experiments were conducted at least three times and error bars represent the SEM.

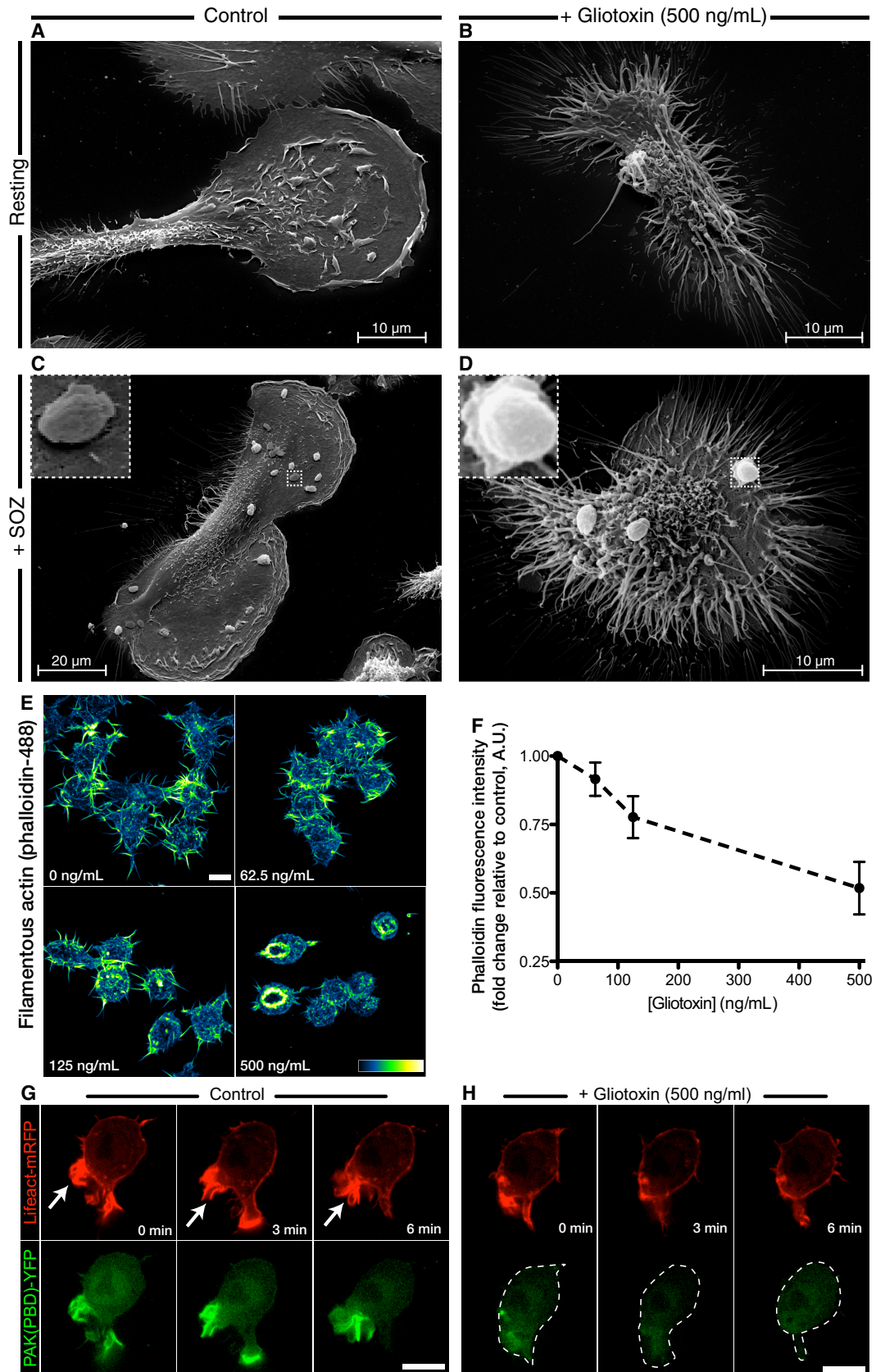


FIG 3 Gliotoxin alters the actin cytoskeleton and Rho GTPase activation. (A to D) Ultrastructural characterization of the morphological changes induced by gliotoxin. Primary human macrophages were treated with DMSO (left panels) or gliotoxin (right panels) for 50 min before being fixed and imaged by scanning (Continued)

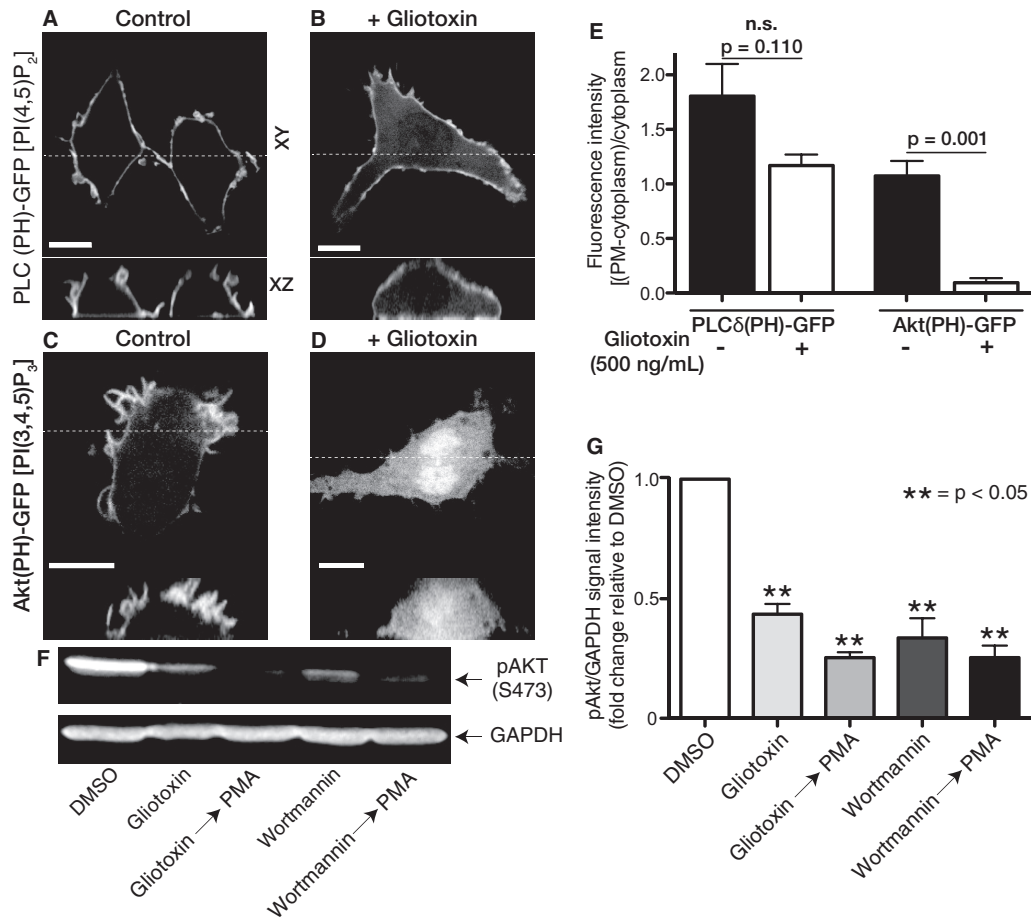


FIG 4 PtdIns(3,4,5) P_3 is depleted in gliotoxin-treated macrophages. (A to D) RAW 264.7 cells transiently expressing PLC δ (PH)-GFP (A and B) or Akt(PH)-GFP (C and D), biosensors for PtdIns(4,5) P_2 and PtdIns(3,4,5) P_3 , respectively. Cells were treated with DMSO (left panels) or 500 ng/ml gliotoxin (right panels) for 30 min immediately before being imaged live by spinning-disk confocal microscopy. Illustrated in each panel are single XY (top) and XZ (bottom) optical slices. The white dotted line along the XY plane indicates the coordinates of the XZ plane. Bars = 10 μ m. (E) Quantification of plasmalemmal fluorescence intensity in DMSO- or gliotoxin-treated macrophages expressing the indicated phosphoinositide biosensor. Values were obtained by dividing the difference between plasmalemmal and cytoplasmic fluorescence by the cytoplasmic fluorescence, thus accounting for differential levels of expression and photobleaching. Values that are not statistically significant (n.s.) are indicated. (F) Macrophage-colony stimulating factor (M-CSF)-dependent phosphorylation of Akt at serine 473 was assessed by immunoblotting as an alternative readout of PtdIns(3,4,5) P_3 abundance. RAW 264.7 cells were first treated for 30 min with DMSO, gliotoxin, or the PI3K inhibitor wortmannin. Where indicated, cells were incubated with PMA following gliotoxin or wortmannin exposure for the last 15 min of treatment. For all conditions in panel F, cells were activated with M-CSF 5 min prior to extraction in order to induce PI3K signaling. pAKT, phosphorylated Akt. (G) Quantification of the phospho-Akt signal divided by that of GAPDH in the immunoblot shown in panel F. Values are reported as changes relative to the DMSO-treated control. Experiments were conducted at least three times, and error bars represent the SEM.

the supplemental material, control macrophages exposed to large targets readily completed phagocytosis of the majority of their contacted targets, as expected. In sharp contrast, internalization of these large targets was precluded in response to gliotoxin

(Fig. S2B). Of note, gliotoxin-treated macrophages developed abortive, actin-rich phagocytic cups akin to those observed in cells with impaired PI3K activity. Gliotoxin treatment also led to a marked reduction in the total number of large targets that were

Figure Legend Continued

electron microscopy. Cells in panels C and D were challenged with serum-opsonized zymosan for the last 20 min of gliotoxin treatment. Insets display magnified views of zymosan particles contacted by control (C) and gliotoxin-treated cells (D). (E) Visualization of the microfilament skeleton of RAW 264.7 cells treated with gliotoxin at the concentrations indicated on each micrograph's lower left. After 30 min of gliotoxin treatment, cells were stained with Alexa Fluor 488-conjugated phalloidin and imaged by spinning-disk confocal microscopy. Images were pseudocolored according to the heat map shown on the bottom right. (F) Quantification of phalloidin fluorescence intensity in the cells shown in panel E as a function of gliotoxin concentration, representative of the relative levels of F-actin. Values have been normalized to the untreated control condition. A.U., arbitrary units. (G and H) Micrographs obtained by time-lapse fluorescence microscopy showing sites of actin polymerization and Rac/Cdc42 activation. RAW 264.7 macrophages were transiently cotransfected with constructs encoding Lifeact-mRFP (top panel) and PAK(PBD)-YFP (bottom panel), fluorescent probes for F-actin and active Rac/Cdc42, respectively. The arrows in panel G point to membrane ruffles formed by untreated cells at sites of Rho GTPase activation. The cells in panel H were exposed to gliotoxin at the 0-min time point. Bars in panels E to H) = 10 μ m. Experiments were conducted at least three times, and error bars represent the standard errors of the means. SOZ, serum-opsonized zymosan.

associated with the macrophages, a phenomenon likely attributed to the inability of gliotoxin-exposed cells to ruffle their membranes and probe their microenvironment. The toxin also caused a decrease in the total number of small targets associated with the macrophage surface. Remarkably, however, gliotoxin did not alter the efficiency with which these small targets were phagocytosed; the majority of small beads contacted by both control and gliotoxin-treated cells were internalized. A quantification of these determinations is provided in Fig. S2E and S2F. Together, these results indicate that gliotoxin profoundly depresses the efficiency of macrophages to phagocytose large, but not small, targets. The differential effect of gliotoxin on the phagocytosis of large versus small targets is in line with the notion of PI3K being a gliotoxin target in professional phagocytes.

PMA promotes PtdIns(3,4,5)P₃-independent ruffling and phagocytosis. While assessing the effect of gliotoxin on integrin activation (see Fig. S3C and S3D in the supplemental material), we made an interesting, serendipitous observation: in response to PMA, gliotoxin-treated macrophages not only activated β_2 integrins well above resting levels (Fig. S3D), they also regained their ability to ruffle and spread their membranes. Figure 5A and Movie S5 in the supplemental material show human monocyte-derived macrophages pretreated with gliotoxin for 15 min and exposed to 100 nM PMA immediately thereafter. Notably, the addition of this diacylglycerol analogue effected the transformation of gliotoxin-induced retraction fibers into highly motile and dynamic peripheral membrane ruffles. Since PMA allowed for gliotoxin-treated macrophages to reestablish their morphology and regain cytoskeletal dynamics, we questioned whether cells treated in this manner also recovered their phagocytic capacity. To investigate this, RAW 264.7 cells that had been treated with gliotoxin for 15 min were subsequently exposed to PMA or vehicle (DMSO) alone for an additional 20 min and then challenged with IgG-opsonized erythrocytes (Fig. 5C and D). As anticipated, the ability to engage and internalize IgG-coated targets by macrophages treated with gliotoxin alone was greatly impaired. More strikingly, however, gliotoxin-treated cells that were subsequently stimulated with PMA regained their ability to engage and internalize IgG-RBC; their phagocytic efficiency did not differ significantly from that of controls (Fig. 5C and D).

That PMA was capable of reversing gliotoxin toxicity suggested that the phorbol ester activated signaling components lying downstream of PtdIns(3,4,5)P₃, which we showed above is a primary target of gliotoxin. If this were the case, then PMA-induced membrane ruffling and phagocytosis in gliotoxin-treated cells should be restored in the absence of plasmalemmal PtdIns(3,4,5)P₃. We tested this premise by electroporating human monocyte-derived macrophages with the PtdIns(3,4,5)P₃ biosensor Akt(PH)-GFP. Transfectants were then treated with gliotoxin and finally stimulated with PMA or not stimulated. As expected, resting macrophages elaborated extensive membrane ruffles that were rich in PtdIns(3,4,5)P₃, and these disappeared upon gliotoxin treatment (Fig. 5B, left and middle panels). In contrast, the membrane ruffles induced by PMA in gliotoxin-treated cells were devoid of PtdIns(3,4,5)P₃ (Fig. 5A and B, right panels). Together, these observations are consistent with the notion that PMA rescues macrophage function from the gliotoxin-mediated insult on PtdIns(3,4,5)P₃ by triggering signaling pathways that operate downstream of this phosphoinositide. Our findings also raise the interesting possibility that a key role of PtdIns(3,4,5)P₃ during the

formation of membrane ruffles and pseudopodia is to signal diacylglycerol biosynthesis.

DISCUSSION

While considering possible gliotoxin targets in immune cells, it is helpful to recall that this is a small, membrane-permeant molecule (12, 49, 50) whose toxicity entirely depends on its bridged disulfide ring (11, 51). Indeed, gliotoxin activity is abolished in the presence of reducing reagents or by substituting the disulfide bridge with a dimethylthioether moiety (19). This, in conjunction with the hydrophobicity of gliotoxin, supports the notion that the mycotoxin operates by modifying host proteins that carry susceptible thiol groups, generating mixed disulfides via disulfide-sulfhydryl exchange. Proteins residing in the cytoplasmic compartment, a reducing environment, are thus likely targets of the toxin. The availability of multiple sulfhydryl-containing proteins in the cytosol implies that several separate targets could be affected by gliotoxin, accounting for its profound immunosuppressive effects. Indeed, previous reports have indicated that this mycotoxin inhibits NADPH oxidase function in neutrophils (14, 52), precludes the cytotoxic properties of T lymphocytes (13), and prevents NF- κ B-dependent transcription of cytokines in both B and T cells (17). A recent study also suggested that gliotoxin induces cytoskeletal abnormalities in neutrophils by elevating the cellular concentration of cAMP (32). However, despite observing similar defects in the actin architecture of macrophages, we failed to detect any alterations in the activity of cAMP effectors in response to the toxin (see Fig. S3 in the supplemental material). Consistent with our inability to detect gliotoxin-induced alterations in cAMP levels, it was previously indicated that the activity of a cAMP-sensing transcription factor (CREB or cAMP response element-binding protein) was not affected in gliotoxin-treated T lymphocytes (17). Thus, the effect of gliotoxin on cAMP may be unique to neutrophils.

Rather than increasing the cAMP content of macrophages, gliotoxin seems to subvert their PtdIns(3,4,5)P₃ metabolism. At present, it is unclear whether the decline in PtdIns(3,4,5)P₃ results from stimulated degradation or from inhibition of its synthesis, and these mechanisms are not mutually exclusive. Regardless of the precise underlying mechanism, the decrease in PtdIns(3,4,5)P₃ can readily account for the gliotoxin-induced cytoskeletal and physiological abnormalities. First, localized accumulation of PtdIns(3,4,5)P₃ is thought to be necessary to assemble the actin-driven projections that underlie membrane ruffling (30, 53) and phagosome formation (23, 24). Accordingly, gliotoxin profoundly affected the ability of macrophages to form peripheral membrane ruffles (see Movies S1, S3, and S4 in the supplemental material) and complete phagocytosis (Fig. 1). Remarkably, the aborted phagocytic cups formed by gliotoxin-treated cells (Fig. 3D) were morphologically similar to those reported in cells treated with PI3K inhibitors (22–24). This too bolsters the notion that gliotoxin interferes with PtdIns(3,4,5)P₃ homeostasis. Second, earlier studies have proposed an essential role for PtdIns(3,4,5)P₃ in the inside-out activation of β_1 and β_2 integrins in immune cells (54–57), and we have provided evidence that gliotoxin prevents activation of β integrins (see Fig. S3C and S3D in the supplemental material). Third, it is well established that 3'-phosphoinositides provide survival signals through Akt (58–61), and as in other cell types (12, 21, 49), we found that a sufficiently long exposure to gliotoxin eventually leads to macrophage

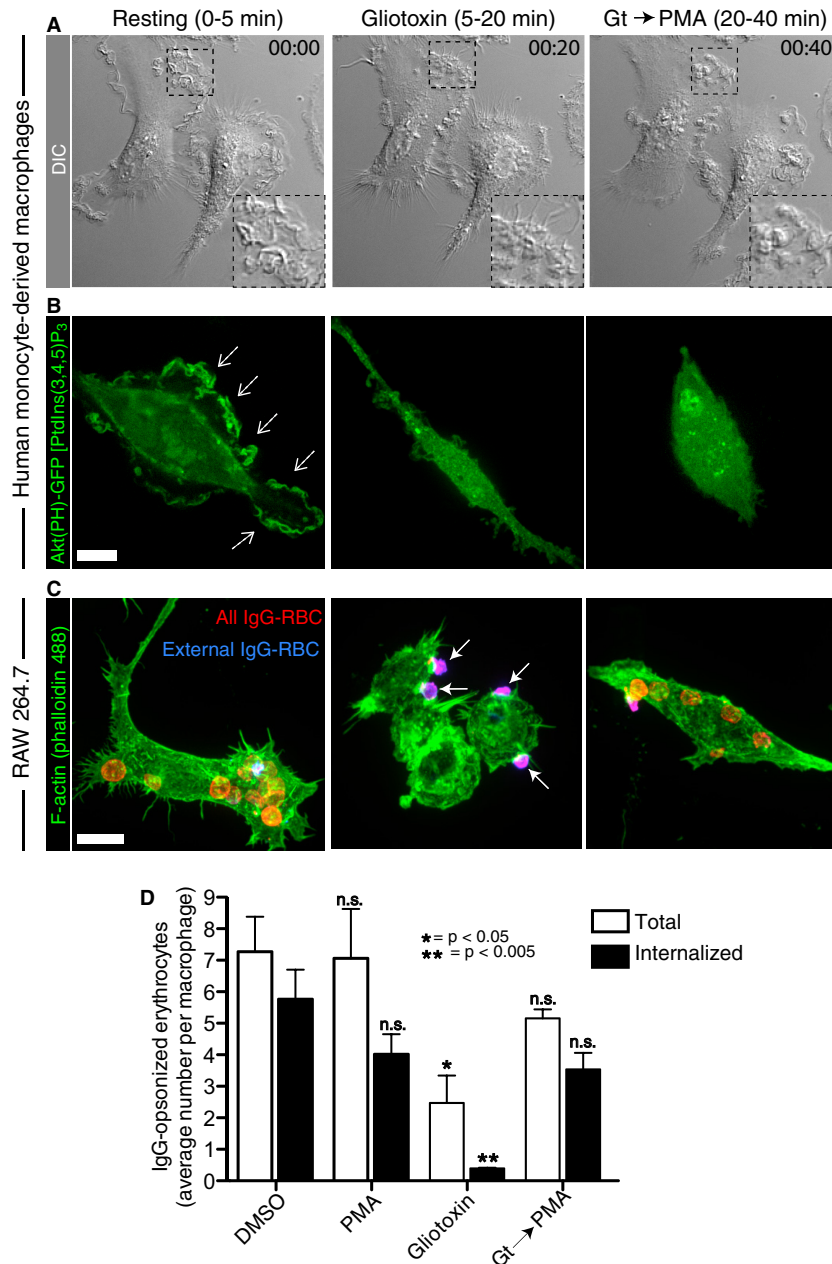


FIG 5 PtdIns(3,4,5)P₃-independent membrane ruffling and phagocytosis in response to PMA. (A and B) Representative micrographs of primary human macrophages imaged live by time-lapse differential interference contrast (DIC) microscopy (A) or confocal microscopy (B). Cells were imaged under resting conditions (0- to 5-min time point), 15 min following gliotoxin exposure (5- to 20-min time point) and 20 min after treatment with PMA (20- to 40-min time point). Gliotoxin was not removed from the medium during the time of PMA activation. The insets in panel A show magnified views of actively ruffling regions under resting conditions (left), the retraction of these extensions upon gliotoxin treatment (middle), and their reappearance in response to PMA activation (right). The primary macrophages in panel B were electroporated with a construct encoding Akt(PH)-GFP, a fluorescent reporter of PtdIns(3,4,5)P₃. Dashed arrows point to sites of PtdIns(3,4,5)P₃ accumulation within extensive membrane ruffles in resting cells. (C) Representative Z-projections of RAW 264.7 cells challenged with IgG-opsonized erythrocytes. Macrophages were treated under the same conditions as the cells in panels A and B, and phagocytosis was initiated immediately thereafter. Ten minutes following exposure to phagocytic targets, cells were fixed and permeabilized, and their F-actin skeleton was stained with Alexa Fluor 488-conjugated phalloidin. All phagocytic particles are shown in red, while those that remained extracellular at the time of fixation are shown in blue. Solid arrows point to abortive phagocytic cups developed in gliotoxin-treated cells. Bars = 10 μ m. (D) Quantification of the total (white bars) and internalized (black bars) number of IgG-opsonized targets associated per macrophage under the indicated conditions. Experiments were conducted at least three times, and error bars represent the SEM. IgG-RBC, IgG-opsonized red blood cells; Gt, gliotoxin.

apoptosis (Fig. S1). Interference with PtdIns(3,4,5)P₃ accumulation provides a unifying hypothesis that provides an explanation for the effects of gliotoxin on phagocytosis, integrin activation, and even cell survival.

Integrin activation and Rho GTPase-mediated actin nucleation are two main components of the phagocytic response. PtdIns(3,4,5)P₃ recruits modulators of Rac activity that possess PH domains, thereby orchestrating the assembly of the actin

meshwork. In turn, actin-based networks generate membrane ruffles that sample the extracellular environment for targets (30, 53) and also propel the formation of pseudopods to engulf such targets (24). The failure of gliotoxin-treated macrophages to activate Rac (Fig. 3) is also expected to hinder the production of microbicidal superoxide anions by the NADPH oxidase, as this Rho GTPase is critical for the assembly and activation of the oxidative complex (62). Thus, by interfering with PtdIns(3,4,5)P₃ levels—and therefore with Rac activation—gliotoxin could preclude the effective deployment of the oxidative complex. That superoxide formation is critical for combating *A. fumigatus* is supported by the observation that IA is the primary cause of death in patients with chronic granulomatous disease, a primary immunodeficiency caused by mutations in NADPH oxidase components. Thus, gliotoxin could exacerbate infection in individuals with a functional NADPH oxidase by interfering with the PtdIns(3,4,5)P₃-Rac-NADPH oxidase axis. It is also likely that the mycotoxin obstructs the phagocytic response by inhibiting the activation of β integrins, which are necessary for optimal phagocytosis (63–65). In this context, it is noteworthy that inside-out integrin activation during phagocytosis is normally dependent on PI3K activity (63, 64).

Strikingly, while PtdIns(3,4,5)P₃ is a key signaling component during the activation of Rho family GTPases and β integrins, we found that PMA treatment restored membrane ruffling in gliotoxin-treated macrophages, which also regained the ability to spread and phagocytose prey in a seemingly PtdIns(3,4,5)P₃-independent manner (Fig. 5). How is this unexpected observation explained? As a diacylglycerol analogue, it is conceivable that PMA directly stimulates the function of calcium- and diacylglycerol-regulated guanine nucleotide exchange factor I (CalDAG-GEFI), a diacylglycerol-regulated GEF that promotes inside-out integrin activation through the Rap1 GTPase (37, 66–69). This would bypass the need to generate diacylglycerol by PtdIns(3,4,5)P₃-tk; 4initiated activation of phospholipase C. Interestingly, active Rap1 has been shown to directly recruit the Rac GEFs Tiam1 and Vav2 to sites of active membrane protrusion (70). Thus, catalyzing nucleotide exchange on Rap1 by CalDAG-GEFI would not only restore integrin function during phagocytosis and spreading; it would also promote the reestablishment of actin cytoskeletal dynamics. Because CalDAG-GEFI, Tiam1, and Vav2 signal downstream of PtdIns(3,4,5)P₃, the PMA-mediated stimulation of these GEFs would bypass the subversion of PtdIns(3,4,5)P₃ by gliotoxin, thus restoring integrin avidity and cytoskeletal dynamics.

While our studies suggest an unequivocal role for gliotoxin in hindering macrophage function *in vitro*, conflicting evidence exists on whether the mycotoxin is necessary for *Aspergillus* virulence *in vivo*. Independent studies in which immunodeficient mice were infected with wild-type or gliotoxin-deficient *Aspergillus* mutants have reached opposing conclusions on whether gliotoxin is necessary for virulence (71–75). However, it has since become apparent that the discrepancy lay on the regime used for immunosuppression: mice that had been rendered neutropenic (through a combination of corticosteroids and cyclophosphamide) were equally susceptible to wild-type and gliotoxin-deficient strains (71, 73, 74), while mice retaining its neutrophil population (those treated with corticosteroids alone) succumbed less easily to infection when gliotoxin was deleted (72, 75–77). Thus, neutrophils seem to be a critical target of gliotoxin toxicity

during *Aspergillus* pathobiology. Given the universal role of PtdIns(3,4,5)P₃ in controlling actin-driven processes such as chemotaxis (31) and phagocytosis (78), it is quite feasible that the mechanisms we describe for macrophages herein apply also to neutrophils. Indeed, dysregulation of PtdIns(3,4,5)P₃ signals could account for the inhibition of phagocytosis and impairment of NADPH oxidase function that has been previously reported in neutrophils (32, 52).

Macrophages and neutrophils thus seem to carry out independent yet complementary tasks in shaping the course of *Aspergillus* pathobiology: the former are responsible for the quick and efficient phagocytosis of inhaled conidia, while the latter may play a more active role in contending with complex and extensive hyphal networks, which are simply too large for macrophages to phagocytose. By subverting phosphoinositide signaling—and therefore interfering with both actin cytoskeletal dynamics and integrin function—gliotoxin may impair the function of both kinds of professional phagocytes, thereby ensuring the survival of its progeny while keeping hyphal networks clear from neutrophil onslaught.

MATERIALS AND METHODS

Plasmids. PAK(PBD)-YFP, the p21-binding domain (PBD) of p21-activated kinase (PAK) conjugated to yellow fluorescent protein (YFP) (31), was used to monitor the subcellular distribution of active (GTP-bound) Rac and Cdc42. The presence of F-actin was visualized in living cells using a construct encoding Lifeact-mRFP. The latter is a mRFP-conjugated, 17-amino-acid peptide derived from the *Saccharomyces cerevisiae* actin-binding protein Abp140 (79). The distributions of PtdIns(4,5)P₂ and phosphatidylinositol 3,4,5-trisphosphate [PtdIns(3,4,5)P₃] were monitored using constructs encoding green fluorescent protein (GFP) chimeras of the pleckstrin homology (PH) domains of phospholipase C δ (PLC δ) (46) or of Akt (47), respectively.

Antibodies. Erythrocyte opsonization was carried out with rabbit anti-sheep red blood cell antibodies (Cedarlane Laboratories). Cy5- and Cy3-conjugated antibodies against rabbit IgG (Jackson ImmunoResearch) were employed to visualize the erythrocyte targets. The levels of cell-surface phagocytic receptors were detected by immunofluorescence and flow cytometry via an Fc γ receptor I (Fc γ RI)-specific rat monoclonal antibody (catalog no. MAB20741; R&D Systems) or with a rat antibody that recognizes an epitope shared by both Fc γ RIIb and Fc γ RIII (catalog no. 14-0161; eBioscience). An isotype-matched rat IgG2a antibody (catalog no. MAB006) was obtained from R&D Systems. Anti-Fc γ R antibodies and the associated isotype control were all employed at final concentrations of 10 μ g/ml. For a secondary antibody, we used anti-rat IgG conjugated to Alexa Fluor 488 (catalog no. 4416; Cell Signaling) at a 1:500 dilution. Sites of integrin β_2 activation were visualized by immunofluorescence with a mouse monoclonal antibody against high-affinity human CD18 (clone MEM-148; Abcam). As an indication of phosphatidylinositol 3-kinase (PI3K) activity, we measured phosphorylation of Akt at serine 473 by immunoblotting, using a rabbit polyclonal antibody (catalog no. 9271S; Cell Signaling). A rabbit polyclonal antibody was used to detect vasodilator-stimulated phosphoprotein (VASP) phosphorylation at serine 157 (catalog no. 3111S; Cell Signaling), a marker of protein kinase A (PKA) activity. An anti-glyceraldehyde-3-phosphate dehydrogenase (GAPDH) mouse monoclonal antibody (catalog no. MAB374; EMD Millipore) was utilized as a loading control. The Western blotting section below details the concentrations and incubation times used.

Cell culture of immortalized and primary macrophages. The immortalized RAW 264.7 murine macrophage line was obtained from the American Type Culture Collection (ATCC) and cultured at 37°C under 5% CO₂ in RPMI 1640 supplemented with 5% heat-inactivated fetal bovine serum (FBS) (Wisent). For the preparation of primary human macrophages, peripheral blood was obtained from healthy donors and diluted

with phosphate-buffered saline (PBS) at a 1:1 ratio. The diluted blood was then resuspended in Lympholyte-H (Cedarlane), and peripheral blood mononuclear cells (PBMCs) were purified by density gradient centrifugation. PBMCs were then allowed to settle onto 1.8-cm glass coverslips at an approximate density of 3×10^6 cells per coverslip. The cells were then cultured for 6 days (37°C, 5% CO₂) in RPMI 1640 supplemented with 10% heat-inactivated FBS (Wisent) and penicillin-streptomycin (Multi-cell). To promote monocyte differentiation, macrophage colony-stimulating factor (25 ng/ml) was added at the onset of culture and every other day throughout the 6 days of culture. Nonadherent cells were washed off the macrophage monolayer at the conclusion of the differentiation period.

Transfection and electroporation. For transient transfections of RAW 264.7 macrophages, almost confluent monolayers were lifted by gentle scraping and plated onto 1.8-cm coverslips (1×10^5 cells per coverslip). Approximately 18 h after plating, cells were transfected with FuGENE HD (Promega) according to the manufacturer's protocol. In short, 6 μ l of the FuGENE HD transfection reagent and 3 μ g of plasmid DNA were mixed in 100 μ l of serum-free RPMI 1640 and allowed to sit for 30 min. The transfection mix was then supplemented with 500 μ l of RPMI 1640 containing 10% heat-inactivated FBS and distributed in equal amounts to 4 wells of a 12-well plate. In the case of human monocyte-derived macrophages, transient expression of fluorescent proteins was attained by electroporation with the Neon transfection system (Life Technologies). Following 5 to 6 days of differentiation in culture, primary macrophages were lifted by exposure to Accutase (Innovative Cell Technologies) and gentle scraping. Next, 5×10^5 macrophages were centrifuged at $300 \times g$ for 5 min before being resuspended in 100 μ l of the supplied buffer R. The cell suspension was then added to 15 μ g of plasmid DNA and subjected to electroporation by two sequential 30-ms pulses of 1,100 V each. To maximize cell survival, electroporated macrophages were immediately transferred to RPMI 1640 supplemented with 10% heat-inactivated FBS before plating onto glass coverslips.

Gliotoxin and other pharmacological treatments. Gliotoxin (Sigma-Aldrich) was diluted in DMSO and utilized at a final concentration of 500 ng/ml (1.53 μ M) in all instances, except for experiments in which the toxin was serially diluted. Gliotoxin was added while the cells were in serum-free medium and allowed to act for 30 min before further experimental manipulations were carried out. In the cases where gliotoxin challenge was followed by the addition of a second compound (e.g., phorbol myristate acetate [PMA]), gliotoxin was not removed from the medium. PMA and wortmannin were both used at 100 nM for the indicated periods. The adenylate cyclase activator forskolin (Sigma-Aldrich) and the competitive inhibitor of cAMP signaling (*R*)-adenosine, cyclic 3',5'-(hydrogenphosphorothioate) trimethylammonium (cAMPS-Rp) (Tocris Bioscience) were utilized at final concentrations of 100 and 200 μ M, respectively. Where indicated, cells were pretreated with cAMPS-Rp before being exposed to either gliotoxin or forskolin.

Phagocytosis. Fc γ R-mediated phagocytosis was studied using either IgG-coated erythrocytes (10% suspension) (MP Biomedicals) or IgG-coated beads (Bangs Laboratories Inc.) as targets for RAW 264.7 macrophages. Opsonization was carried out by mixing 200 μ l of the erythrocyte suspension with 5 μ l of a rabbit anti-sheep erythrocyte IgG or by diluting divinylbenzene (DVB)-coated polystyrene beads 10-fold in PBS and mixing them with human IgG (final concentration, 5 mg/ml) at room temperature for 1 h under constant agitation. Unbound IgG was removed by washing the particles three times with PBS. Opsonized targets were subsequently labeled with a Cy3-conjugated IgG, and excess antibody was removed by washing the particles twice with PBS before resuspending them in 200 μ l of PBS. To initiate phagocytosis, 10 μ l of the IgG-coated erythrocyte suspension or 15 μ l of the bead suspension was added to 2×10^5 RAW 264.7 cells and centrifuged at $300 \times g$ for 30 s. Phagocytosis was allowed to proceed for 30 min before the cells were fixed with 4% paraformaldehyde (PFA). Extracellular targets were identified by incubating the fixed (nonpermeabilized) cells with a Cy5-conjugated anti-rabbit an-

tibody. Alternatively, phagocytosis of fungal particles by primary macrophages was analyzed with zymosan A bioparticles (Molecular Probes) as phagocytic targets. Lyophilized zymosan was suspended in PBS (20 mg/ml), boiled for 1 h, and subjected to three cycles of vortexing and sonication. The solution was then diluted to 2 mg/ml in PBS at pH 9 and further homogenized by passing through a syringe 10 times. The particles were then simultaneously labeled with succinimidyl esters of Alexa Fluor 555 (Invitrogen) and of biotin (Thermo Fisher Scientific), according to the manufacturers' instructions. Excess dye and biotin were removed by centrifuging and washing twice with PBS. Labeled zymosan was left unopsonized or coated with human serum. For the latter, 500 μ l of the 2-mg/ml zymosan suspension was diluted 1:1 with human serum and incubated for 1 h with constant agitation at 37°C. The primary macrophages were challenged with 1 mg/ml unopsonized or serum-opsonized zymosan (5 μ l per coverslip), and phagocytosis was terminated after 30 min by bathing the cells in HBSS at 15°C. Extracellular targets were identified by exposing the macrophages to an Alexa Fluor 647 conjugate of streptavidin for 15 min at 15°C, which labeled the biotin tag on zymosan. Last, macrophages were fixed for 15 min in 4% PFA, and permeabilized with 0.1% Triton X-100 for 5 min, and their F-actin skeleton was stained with Alexa Fluor 488-conjugated phalloidin for 30 min.

IgG-binding assays. Fc γ R affinity was assessed by measuring the binding of fluorescent IgG aggregates to the surfaces of RAW 264.7 macrophages. To form the aggregates, a 10-mg/ml solution of human IgG and Cy3-conjugated donkey IgG was agitated for 30 min at 62°C in PBS with Ca²⁺ and Mg²⁺. Insoluble aggregates were removed by spinning down at $1,600 \times g$ for 10 min. The supernatant was added to macrophages grown on 1.8-cm coverslips (20 μ l of supernatant/ml of culture medium), and binding was allowed to proceed for 15 min at 10°C to prevent IgG internalization. Cells were then washed twice with PBS, fixed in 4% PFA for 20 min, and imaged by confocal microscopy. Integrated fluorescence was used as an indication of binding affinity.

Microscopy and image analysis. Fluorescence imaging was performed by spinning-disk confocal microscopy (Quorum Technologies). Our confocal systems are based on an Axiovert 200M microscope (Carl Zeiss) and carry a 63 \times oil-immersion objective with a 1.4 numerical aperture (NA) and a 1.5 \times magnifying lens. These microscopes are equipped with a motorized XY stage (Applied Scientific Instrumentation), a Piezo Z-focus drive and diode-pumped solid-state lasers emitting at 440, 491, 561, 638, and 655 nm (Spectral Applied Research). Images were recorded with back-thinned, cooled charge-coupled-device cameras (Hamamatsu Photonics) operating under control of the Velocity software (PerkinElmer, version 6.2.1). For time-lapse imaging by differential interference contrast, coverslips were loaded onto Leiden chambers, mounted on the stage of a DM IRB Leica microscope, and maintained at 37°C throughout image acquisition. Cells were illuminated via an XFO X-Cite 120 lamp (XFO Life Sciences Group), and the signal was captured by a cooled charge-coupled-device camera (Cascade II; Photometrics) driven by Velocity (PerkinElmer, version 6.2.1). In preparation for scanning electron microscopy, primary macrophages were fixed in a 2% glutaraldehyde solution buffered with sodium cacodylate. Cells were then dehydrated through a graded ethanol series and dried in a Bal-tec CPD030 critical-point dryer. Last, samples were mounted on aluminum stubs and coated with gold using a Denton Desk II sputter coater. Images were acquired with an FEI XL30 scanning electron microscope. ImageJ (National Institutes of Health, software version 1.48) was used for quantifying fluorescence intensity and correcting brightness and contrast. Adjustments were made homogeneously across the entire image, and the linearity of mapped pixel values was not altered.

Flow cytometry and immunofluorescence. RAW 264.7 macrophages were treated with gliotoxin or vehicle (DMSO) alone in serum-free RPMI 1640 for 30 min. The cells were then lifted from 6-well dishes by gentle scraping and resuspended in 15°C PBS with bovine serum albumin (BSA) (5%) at a density of 1×10^7 cells/ml. Next, the cells were incubated with primary antibodies against Fc γ R or with an isotype-matched rat IgG2a for

1 h on ice. Anti-FcγR antibodies and the associated IgG isotype control were all employed at final concentrations of 10 μg/ml. Excess primary antibody was removed by centrifuging and washing twice with cold PBS. Cells were then incubated with an Alexa Fluor 488-conjugated anti-rat IgG (1:500 final dilution) for 30 min at 15°C, washed with cold PBS, and fixed in 4% PFA. Last, labeled cells were passed through a cell strainer and ran in the flow cytometer (LSRII; BD Biosciences). Analysis was performed in FlowJo (Tree Star, Inc.). For immunofluorescence assays, approximately 1 × 10⁵ RAW 264.7 macrophages were plated on 1.8-cm coverslips and cultured overnight. The cells were then switched to serum-free RPMI 1640 for treatment with gliotoxin. Following 30 min of gliotoxin incubation, the cells were fixed in 4% PFA, blocked in PBS supplemented with BSA (5%), and incubated with primary and secondary antibodies at the same concentrations as those employed for flow cytometry.

Western blotting. For each condition, RAW 264.7 macrophages were plated on 2 wells of a 6-well plate (2.5 × 10⁵ cells/well) and cultured overnight. Cells were then exposed to gliotoxin or to the indicated pharmacological agents, washed with cold PBS, and lifted by scraping in cold radioimmunoprecipitation assay (RIPA) buffer supplemented with protease and phosphatase inhibitors (Roche). Nuclei and cell debris were pelleted by centrifugation. A total of 30 μg of protein from the supernatant was loaded into each lane of a 12% sodium dodecyl sulfate-polyacrylamide gel (SDS-PAGE) and separated by electrophoresis. The proteins were then transferred to polyvinylidene fluoride membranes and blocked for 30 min with 5% bovine serum albumin in Tris-buffered saline (TBS) supplemented with Tween 20 (0.1%). This solution was also used to dilute the antibodies against GAPDH, phospho-Akt (serine 473), and phospho-VASP (serine 157). The anti-GAPDH antibody was employed at a 1:1,000 dilution, while those against phospho-Akt and phospho-VASP were diluted 10,000 times. In all instances, the membranes were incubated with primary antibodies for 1.5 h and washed with TBS-Tween before being exposed to secondary antibodies (diluted 10,000 times) for 45 min. A horseradish peroxidase (HRP)-conjugated goat anti-rabbit secondary antibody was used to detect phospho-Akt and phospho-VASP, while GAPDH was detected with an IRDye 800CW-conjugated donkey anti-mouse secondary antibody (LI-COR, Inc.), also diluted 10,000 times. Membranes were visualized digitally on the Odyssey Fc system (LI-COR, Inc.) after being treated with the enhanced chemiluminescence (ECL) Western blotting substrate (GE Life Sciences). The intensity of independent bands was quantified using the LI-COR Image Studio software and normalized to GAPDH. Brightness and contrast were adjusted evenly across the entire image.

Statistical analysis. Data values are presented as means of three independent replicates, and error bars represent the standard error of the mean (SEM). For microscopy-based determinations, sample sizes were of at least 20 cells and 100 phagosomes per individual experiment. The significance of differences was assessed by unpaired Student's *t* tests with a 95% confidence interval, using GraphPad Prism 5c (GraphPad Software, Inc.).

SUPPLEMENTAL MATERIAL

Supplemental material for this article may be found at <http://mbio.asm.org/lookup/suppl/doi:10.1128/mBio.02242-15/-/DCSupplemental>.

- Figure S1, PDF file, 1.6 MB.
- Figure S2, PDF file, 1.7 MB.
- Figure S3, PDF file, 0.9 MB.
- Movie S1, MOV file, 7.8 MB.
- Movie S2, MOV file, 11.8 MB.
- Movie S3, MOV file, 7.7 MB.
- Movie S4, MOV file, 17.8 MB.
- Movie S5, MOV file, 2.1 MB.

ACKNOWLEDGMENTS

We thank Doug Holmyard for assisting with sample preparation and imaging during experiments involving scanning electron microscopy.

FUNDING INFORMATION

This work, including the efforts of Gregory D. Fair, was funded by Canadian Institutes of Health Research (CIHR) (MOP-133656). This work, including the efforts of Sergio Grinstein, was funded by Canadian Institutes of Health Research (CIHR) (FDN-143202).

D.S. was supported by a Cystic Fibrosis Canada graduate studentship and is currently funded by a Restracom studentship from The Hospital for Sick Children. J.C. is a Cystic Fibrosis Canada postdoctoral fellow. S.A.F. is funded by a fellowship from the Heart and Stroke Foundation of Canada. This work was supported by the Canadian Institutes of Health Research grants FDN-143202 and MOP-133656, awarded to S.G. and G.D.F., respectively. None of the funding agencies listed above had any influence on the design or interpretation of the experiments here described, or in the submission of this manuscript for publication.

REFERENCES

1. Lin SJ, Schranz J, Teutsch SM. 2001. Aspergillus case-fatality rate: systematic review of the literature. *Clin Infect Dis* 32:358–366. <http://dx.doi.org/10.1086/318483>.
2. Denning DW. 1998. Invasive aspergillosis. *Clin Infect Dis* 26:781–805. <http://dx.doi.org/10.1086/513943>.
3. Hauser AR, Jain M, Bar-Meir M, McColley SA. 2011. Clinical significance of microbial infection and adaptation in cystic fibrosis. *Clin Microbiol Rev* 24:29–70. <http://dx.doi.org/10.1128/CMR.00036-10>.
4. Bakare N, Rickerts V, Bargon J, Just-Nübling G. 2003. Prevalence of *Aspergillus fumigatus* and other fungal species in the sputum of adult patients with cystic fibrosis. *Mycoses* 46:19–23. <http://dx.doi.org/10.1046/j.1439-0507.2003.00830.x>.
5. Dagenais TRT, Keller NP. 2009. Pathogenesis of *Aspergillus fumigatus* in invasive aspergillosis. *Clin Microbiol Rev* 22:447–465. <http://dx.doi.org/10.1128/CMR.00055-08>.
6. Tashiro T, Izumikawa K, Tashiro M, Takazono T, Morinaga Y, Yamamoto K, Imamura Y, Miyazaki T, Seki M, Kakeya H, Yamamoto Y, Yanagihara K, Yasuoka A, Kohno S. 2011. Diagnostic significance of *Aspergillus* species isolated from respiratory samples in an adult pneumology ward. *Med Mycol* 49:581–587. <http://dx.doi.org/10.3109/13693786.2010.548084>.
7. Hospenthal DR, Kwon-Chung KJ, Bennett JE. 1998. Concentrations of airborne *Aspergillus* compared to the incidence of invasive aspergillosis: lack of correlation. *Med Mycol* 36:165–168. <http://dx.doi.org/10.1080/02681219880000241>.
8. Schaffner A, Douglas H, Braude AI, Davis CE. 1983. Killing of *Aspergillus* spores depends on the anatomical source of the macrophage. *Infect Immun* 42:1109–1115.
9. Merkow LP, Epstein SM, Sidransky H, Verney E, Pardo M. 1971. The pathogenesis of experimental pulmonary aspergillosis. An ultrastructural study of alveolar macrophages after phagocytosis of *A. flavus* spores in vivo. *Am J Pathol* 62:57–74.
10. Schaffner A, Douglas H, Braude A. 1982. Selective protection against conidia by mononuclear and against mycelia by polymorphonuclear phagocytes in resistance to *Aspergillus*. *J Clin Invest* 69:617–631. <http://dx.doi.org/10.1172/JCI110489>.
11. Gardiner DM, Waring P, Howlett BJ. 2005. The epipolythiodioxopiperazine (ETP) class of fungal toxins: distribution, mode of action, functions and biosynthesis. *Microbiology* 151:1021–1032. <http://dx.doi.org/10.1099/mic.0.27847-0>.
12. Stanzani M, Orciuolo E, Lewis R, Kontoyiannis DP, Martins SLR, St John LS, Komanduri KV. 2005. *Aspergillus fumigatus* suppresses the human cellular immune response via gliotoxin-mediated apoptosis of monocytes. *Blood* 105:2258–2265. <http://dx.doi.org/10.1182/blood-2004-09-3421>.
13. Yamada A, Kataoka T, Nagai K. 2000. The fungal metabolite gliotoxin: immunosuppressive activity on CTL-mediated cytotoxicity. *Immunol Lett* 71:27–32. [http://dx.doi.org/10.1016/S0165-2478\(99\)00155-8](http://dx.doi.org/10.1016/S0165-2478(99)00155-8).
14. Tsunawaki S, Yoshida LS, Nishida S, Kobayashi T, Shimoyama T. 2004. Fungal metabolite gliotoxin inhibits assembly of the human respiratory burst NADPH oxidase. *Infect Immun* 72:3373–3382. <http://dx.doi.org/10.1128/IAI.72.6.3373-3382.2004>.
15. Sutton P, Newcombe NR, Waring P, Müllbacher A. 1994. In vivo

- immunosuppressive activity of gliotoxin, a metabolite produced by human pathogenic fungi. *Infect Immun* 62:1192–1198.
16. Kupfahl C, Geginat G, Hof H. 2006. Gliotoxin-mediated suppression of innate and adaptive immune functions directed against *Listeria monocytogenes*. *Med Mycol* 44:591–599. <http://dx.doi.org/10.1080/13693780600815411>.
 17. Pahl HL, Krauss B, Schulze-Osthoff K, Decker T, Traenckner EB, Vogt M, Myers C, Parks T, Warring P, Mühlbacher A, Czernilofsky AP, Baeuerle PA. 1996. The immunosuppressive fungal metabolite gliotoxin specifically inhibits transcription factor NF-kappaB. *J Exp Med* 183:1829–1840. <http://dx.doi.org/10.1084/jem.183.4.1829>.
 18. Sutton P, Waring P, Müllbacher A. 1996. Exacerbation of invasive aspergillosis by the immunosuppressive fungal metabolite, gliotoxin. *Immunol Cell Biol* 74:318–322. <http://dx.doi.org/10.1038/icb.1996.57>.
 19. Müllbacher A, Waring P, Tiwari-Palni U, Eichner RD. 1986. Structural relationship of epipolythiodioxopiperazines and their immunomodulating activity. *Mol Immunol* 23:231–235. [http://dx.doi.org/10.1016/0161-5890\(86\)90047-7](http://dx.doi.org/10.1016/0161-5890(86)90047-7).
 20. Lewis RE, Wiederhold NP, Chi J, Han XY, Komanduri KV, Kontoyannis DP, Prince RA. 2005. Detection of gliotoxin in experimental and human aspergillosis. *Infect Immun* 73:635–637. <http://dx.doi.org/10.1128/IAI.73.1.635-637.2005>.
 21. Pardo J, Urban C, Galvez EM, Ekert PG, Müller U, Kwon-Chung J, Lobigs M, Müllbacher A, Wallich R, Borner C, Simon MM. 2006. The mitochondrial protein Bak is pivotal for gliotoxin-induced apoptosis and a critical host factor of *Aspergillus fumigatus* virulence in mice. *J Cell Biol* 174:509–519. <http://dx.doi.org/10.1083/jcb.200604044>.
 22. Cox D, Tseng C-C, Bjekic G, Greenberg S. 1999. A requirement for phosphatidylinositol 3-kinase in pseudopod extension. *J Biol Chem* 274:1240–1247. <http://dx.doi.org/10.1074/jbc.274.3.1240>.
 23. Beemiller P, Zhang Y, Mohan S, Levinsohn E, Gaeta I, Hoppe AD, Swanson JA. 2010. A Cdc42 activation cycle coordinated by PI 3-kinase during Fc receptor-mediated phagocytosis. *Mol Biol Cell* 21:470–480. <http://dx.doi.org/10.1091/mbc.E08-05-0494>.
 24. Schlam D, Bagshaw RD, Freeman SA, Collins RF, Pawson T, Fairn GD, Grinstein S. 2015. Phosphoinositide 3-kinase enables phagocytosis of large particles by terminating actin assembly through Rac/Cdc42 GTPase-activating proteins. *Nat Commun* 6:8623. <http://dx.doi.org/10.1038/ncomms9623>.
 25. Park H, Cox D. 2009. Cdc42 regulates Fc gamma receptor-mediated phagocytosis through the activation and phosphorylation of Wiskott-Aldrich syndrome protein (WASP) and neural-WASP. *Mol Biol Cell* 20:4500–4508. <http://dx.doi.org/10.1091/mbc.E09-03-0230>.
 26. Cox D, Chang P, Zhang Q, Reddy PG, Bokoch GM, Greenberg S. 1997. Requirements for both Rac1 and Cdc42 in membrane ruffling and phagocytosis in leukocytes. *J Exp Med* 186:1487–1494. <http://dx.doi.org/10.1084/jem.186.9.1487>.
 27. Hoppe AD, Swanson JA. 2004. Cdc42, Rac1, and Rac2 display distinct patterns of activation during phagocytosis. *Mol Biol Cell* 15:3509–3519. <http://dx.doi.org/10.1091/mbc.E03-11-0847>.
 28. Niedergang F, Chavrier P. 2005. Regulation of phagocytosis by Rho GTPases. *Curr Top Microbiol Immunol* 291:43–60.
 29. Chimini G, Chavrier P. 2000. Function of Rho family proteins in actin dynamics during phagocytosis and engulfment. *Nat Cell Biol* 2:E191–E196. <http://dx.doi.org/10.1038/35036454>.
 30. Bohdanowicz M, Schlam D, Hermansson M, Rizzuti D, Fairn GD, Ueyama T, Somerharju P, Du G, Grinstein S. 2013. Phosphatidic acid is required for the constitutive ruffling and macropinocytosis of phagocytes. *Mol Biol Cell* 24:1700–1712, S1–S7. <http://dx.doi.org/10.1091/mbc.E12-11-0789>.
 31. Srinivasan S, Wang F, Glavas S, Ott A, Hofmann F, K, Kalman D, Bourne HR. 2003. Rac and Cdc42 play distinct roles in regulating PI(3,4,5)P3 and polarity during neutrophil chemotaxis. *J Cell Biol* 160:375–385. <http://dx.doi.org/10.1083/jcb.200208179>.
 32. Coméra C, André K, Laffitte J, Collet X, Galtier P, Maridonneau-Parini I. 2007. Gliotoxin from *Aspergillus fumigatus* affects phagocytosis and the organization of the actin cytoskeleton by distinct signalling pathways in human neutrophils. *Microbes Infect* 9:47–54. <http://dx.doi.org/10.1016/j.micinf.2006.10.009>.
 33. Reinhard M, Halbrügge M, Scheer U, Wiegand C, Jockusch BM, Walter U. 1992. The 46/50 kDa phosphoprotein VASP purified from human platelets is a novel protein associated with actin filaments and focal contacts. *EMBO J* 11:2063–2070.
 34. Lawrence DW, Pryzwansky KB. 2001. The vasodilator-stimulated phosphoprotein is regulated by cyclic GMP-dependent protein kinase during neutrophil spreading. *J Immunol* 166:5550–5556. <http://dx.doi.org/10.4049/jimmunol.166.9.5550>.
 35. Seamon KB, Daly JW. 1986. Forskolin: its biological and chemical properties. *Adv Cyclic Nucleotide Protein Phosphor Res* 20:1–150.
 36. Laurenza A, Sutkowski EM, Seamon KB. 1989. Forskolin: a specific stimulator of adenyl cyclase or a diterpene with multiple sites of action? *Trends Pharmacol Sci* 10:442–447. [http://dx.doi.org/10.1016/S0165-6147\(89\)80008-2](http://dx.doi.org/10.1016/S0165-6147(89)80008-2).
 37. Kawasaki H, Springett GM, Mochizuki N, Toki S, Nakaya M, Matsuda M, Housman DE, Graybiel AM. 1998. A family of cAMP-binding proteins that directly activate Rap1. *Science* 282:2275–2279. <http://dx.doi.org/10.1126/science.282.5397.2275>.
 38. Shimonaka M, Katagiri K, Nakayama T, Fujita N, Tsuruo T, Yoshie O, Kinashi T. 2003. Rap1 translates chemokine signals to integrin activation, cell polarization, and motility across vascular endothelium under flow. *J Cell Biol* 161:417–427. <http://dx.doi.org/10.1083/jcb.200301133>.
 39. Levin R, Grinstein S, Schlam D. 2015. Phosphoinositides in phagocytosis and macropinocytosis. *Biochim Biophys Acta* 1851:805–823. <http://dx.doi.org/10.1016/j.bbali.2014.09.005>.
 40. Raucher D, Stauffer T, Chen W, Shen K, Guo S, York JD, Sheetz MP, Meyer T. 2000. Phosphatidylinositol 4,5-bisphosphate functions as a second messenger that regulates cytoskeleton-plasma membrane adhesion. *Cell* 100:221–228. [http://dx.doi.org/10.1016/S0092-8674\(00\)81560-3](http://dx.doi.org/10.1016/S0092-8674(00)81560-3).
 41. Rohatgi R, Ho HY, Kirschner MW. 2000. Mechanism of N-WASP activation by CDC42 and phosphatidylinositol 4,5-bisphosphate. *J Cell Biol* 150:1299–1310. <http://dx.doi.org/10.1083/jcb.150.6.1299>.
 42. Sechi AS, Wehland J. 2000. The actin cytoskeleton and plasma membrane connection: PtdIns(4,5)P(2) influences cytoskeletal protein activity at the plasma membrane. *J Cell Sci* 113:3685–3695.
 43. Rohatgi R, Nollau P, Ho HY, Kirschner MW, Mayer BJ. 2001. Nck and phosphatidylinositol 4,5-bisphosphate synergistically activate actin polymerization through the N-WASP-Arp2/3 pathway. *J Biol Chem* 276:26448–26452. <http://dx.doi.org/10.1074/jbc.M103856200>.
 44. Das B, Shu X, Day GJ, Han J, Krishna UM, Falck JR, Broek D. 2000. Control of intramolecular interactions between the pleckstrin homology and Dbl homology domains of Vav and Sos1 regulates Rac binding. *J Biol Chem* 275:15074–15081. <http://dx.doi.org/10.1074/jbc.M907269199>.
 45. Ceccarelli DFJ, Blasutig IM, Goudreaux M, Li Z, Ruston J, Pawson T, Sicheri F. 2007. Non-canonical interaction of phosphoinositides with pleckstrin homology domains of Tiam1 and ArhGAP9. *J Biol Chem* 282:13864–13874. <http://dx.doi.org/10.1074/jbc.M700505200>.
 46. Botelho RJ, Teruel M, Dierckman R, Anderson R, Wells A, York JD, Meyer T, Grinstein S. 2000. Localized biphasic changes in phosphatidylinositol-4,5-bisphosphate at sites of phagocytosis. *J Cell Biol* 151:1353–1368. <http://dx.doi.org/10.1083/jcb.151.7.1353>.
 47. Marshall JG, Booth JW, Stambolic V, Mak T, Balla T, Schreiber AD, Meyer T, Grinstein S. 2001. Restricted accumulation of phosphatidylinositol 3-kinase products in a plasmalemmal subdomain during Fc gamma receptor-mediated phagocytosis. *J Cell Biol* 153:1369–1380. <http://dx.doi.org/10.1083/jcb.153.7.1369>.
 48. Burgering BM, Coffey PJ. 1995. Protein kinase B (c-Akt) in phosphatidylinositol-3-OH kinase signal transduction. *Nature* 376:599–602. <http://dx.doi.org/10.1038/376599a0>.
 49. Kweon Y-O, Paik Y-H, Schnabl B, Qian T, Lemasters JJ, Brenner DA. 2003. Gliotoxin-mediated apoptosis of activated human hepatic stellate cells. *J Hepatol* 39:38–46. [http://dx.doi.org/10.1016/S0168-8278\(03\)00178-8](http://dx.doi.org/10.1016/S0168-8278(03)00178-8).
 50. Salvi M, Bozac A, Toninello A. 2004. Gliotoxin induces Mg2+ efflux from intact brain mitochondria. *Neurochem Int* 45:759–764. <http://dx.doi.org/10.1016/j.neuint.2004.01.001>.
 51. Ward C, Chilvers ER, Lawson MF, Pryde JG, Fujihara S, Farrow SN, Haslett C, Rossi AG. 1999. NF-kappaB activation is a critical regulator of human granulocyte apoptosis in vitro. *J Biol Chem* 274:4309–4318. <http://dx.doi.org/10.1074/jbc.274.7.4309>.
 52. Yoshida LS, Abe S, Tsunawaki S. 2000. Fungal gliotoxin targets the onset of superoxide-generating NADPH oxidase of human neutrophils. *Biochem Biophys Res Commun* 268:716–723. <http://dx.doi.org/10.1006/bbrc.2000.2192>.
 53. Flannagan RS, Harrison RE, Yip CM, Jaqaman K, Grinstein S. 2010. Dynamic macrophage “probing” is required for the efficient capture of

- phagocytic targets. *J Cell Biol* 191:1205–1218. <http://dx.doi.org/10.1083/jcb.201007056>.
54. Zell T, Hunt SW, Mobley JL, Finkelstein LD, Shimizu Y. 1996. CD28-mediated up-regulation of beta 1-integrin adhesion involves phosphatidylinositol 3-kinase. *J Immunol* 156:883–886.
 55. Shimizu Y, Mobley JL, Finkelstein LD, Chan AS. 1995. A role for phosphatidylinositol 3-kinase in the regulation of beta 1 integrin activity by the CD2 antigen. *J Cell Biol* 131:1867–1880. <http://dx.doi.org/10.1083/jcb.131.6.1867>.
 56. Kinashi T. 2005. Intracellular signalling controlling integrin activation in lymphocytes. *Nat Rev Immunol* 5:546–559. <http://dx.doi.org/10.1038/nri1646>.
 57. Kolanus W, Nagel W, Schiller B, Zeitlmann L, Godar S, Stockinger H, Seed B. 1996. Alpha L beta 2 integrin/LFA-1 binding to ICAM-1 induced by cytohesin-1, a cytoplasmic regulatory molecule. *Cell* 86:233–242. [http://dx.doi.org/10.1016/S0092-8674\(00\)80095-1](http://dx.doi.org/10.1016/S0092-8674(00)80095-1).
 58. Millburn CC, Deak M, Kelly SM, Price NC, Alessi DR, Van Aalten DMF. 2003. Binding of phosphatidylinositol 3,4,5-trisphosphate to the pleckstrin homology domain of protein kinase B induces a conformational change. *Biochem J* 375:531–538. <http://dx.doi.org/10.1042/BJ20031229>.
 59. Thomas CC, Deak M, Alessi DR, van Aalten DMF. 2002. High-resolution structure of the pleckstrin homology domain of protein kinase B/Akt bound to phosphatidylinositol (3,4,5)-trisphosphate. *Curr Biol* 12:1256–1262. [http://dx.doi.org/10.1016/S0960-9822\(02\)00972-7](http://dx.doi.org/10.1016/S0960-9822(02)00972-7).
 60. Calleja V, Alcor D, Laguerre M, Park J, Vojnovic B, Hemmings BA, Downward J, Parker PJ, Larijani B. 2007. Intramolecular and intermolecular interactions of protein kinase B define its activation in vivo. *PLoS Biol* 5:e95. <http://dx.doi.org/10.1371/journal.pbio.0050095>.
 61. Hers I, Vincent EE, Tavaré JM. 2011. Akt signalling in health and disease. *Cell Signal* 23:1515–1527. <http://dx.doi.org/10.1016/j.cellsig.2011.05.004>.
 62. Dinauer MC. 2003. Regulation of neutrophil function by Rac GTPases. *Curr Opin Hematol* 10:8–15. <http://dx.doi.org/10.1097/00062752-200301000-00003>.
 63. Flannagan RS, Canton J, Furuya W, Glogauer M, Grinstein S. 2014. The phosphatidylserine receptor TIM4 utilizes integrins as coreceptors to effect phagocytosis. *Mol Biol Cell* 25:1511–1522. <http://dx.doi.org/10.1091/mbc.E13-04-0212>.
 64. Jongstra-Bilen J, Harrison R, Grinstein S. 2003. Fcγ-receptors induce Mac-1 (CD11b/CD18) mobilization and accumulation in the phagocytic cup for optimal phagocytosis. *J Biol Chem* 278:45720–45729. <http://dx.doi.org/10.1074/jbc.M303704200>.
 65. Vachon E, Martin R, Kwok V, Cherepanov V, Chow C-W, Doerschuk CM, Plumb J, Grinstein S, Downey GP. 2007. CD44-mediated phagocytosis induces inside-out activation of complement receptor-3 in murine macrophages. *Blood* 110:4492–4502. <http://dx.doi.org/10.1182/blood-2007-02-076539>.
 66. Clyde-Smith J, Silins G, Gartside M, Grimmond S, Etheridge M, Apolloni A, Hayward N, Hancock JF. 2000. Characterization of Ras-GRP2, a plasma membrane-targeted, dual specificity Ras/Rap exchange factor. *J Biol Chem* 275:32260–32267. <http://dx.doi.org/10.1074/jbc.M006087200>.
 67. Ghandour H, Cullere X, Alvarez A, Luscinikas FW, Mayadas TN. 2007. Essential role for Rap1 GTPase and its guanine exchange factor CalDAG-GEFI in LFA-1 but not VLA-4 integrin mediated human T-cell adhesion. *Blood* 110:3682–3690. <http://dx.doi.org/10.1182/blood-2007-03-077628>.
 68. Crittenden JR, Bergmeier W, Zhang Y, Piffath CL, Liang Y, Wagner DD, Housman DE, Graybiel AM. 2004. CalDAG-GEFI integrates signaling for platelet aggregation and thrombus formation. *Nat Med* 10:982–986. <http://dx.doi.org/10.1038/nm1098>.
 69. Pasvolovsky R, Feigelson SW, Kilic SS, Simon AJ, Tal-Lapidot G, Grabovsky V, Crittenden JR, Amariglio N, Safran M, Graybiel AM, Rechavi G, Ben-Dor S, Etzioni A, Alon R. 2007. A LAD-III syndrome is associated with defective expression of the Rap-1 activator CalDAG-GEFI in lymphocytes, neutrophils, and platelets. *J Exp Med* 204:1571–1582. <http://dx.doi.org/10.1084/jem.20070058>.
 70. Arthur WT, Quilliam LA, Cooper JA. 2004. Rap1 promotes cell spreading by localizing Rac guanine nucleotide exchange factors. *J Cell Biol* 167:111–122. <http://dx.doi.org/10.1083/jcb.200404068>.
 71. Bok JW, Chung D, Balajee SA, Marr KA, Andes D, Nielsen KF, Frisvad JC, Kirby KA, Keller NP. 2006. GliZ, a transcriptional regulator of gliotoxin biosynthesis, contributes to *Aspergillus fumigatus* virulence. *Infect Immun* 74:6761–6768. <http://dx.doi.org/10.1128/IAI.00780-06>.
 72. Bok JW, Balajee SA, Marr KA, Andes D, Nielsen KF, Frisvad JC, Keller NP. 2005. LaeA, a regulator of morphogenetic fungal virulence factors. *Eukaryot Cell* 4:1574–1582. <http://dx.doi.org/10.1128/EC.4.9.1574-1582.2005>.
 73. Cramer RA, Gamcsik MP, Brooking RM, Najvar LK, Kirkpatrick WR, Patterson TF, Balibar CJ, Graybill JR, Perfect JR, Abraham SN, Steinbach WJ. 2006. Disruption of a nonribosomal peptide synthetase in *Aspergillus fumigatus* eliminates gliotoxin production. *Eukaryot Cell* 5:972–980. <http://dx.doi.org/10.1128/EC.00049-06>.
 74. Kupfahl C, Heinekamp T, Geginat G, Ruppert T, Härtl A, Hof H, Brakhage AA. 2006. Deletion of the gliP gene of *Aspergillus fumigatus* results in loss of gliotoxin production but has no effect on virulence of the fungus in a low-dose mouse infection model. *Mol Microbiol* 62:292–302. <http://dx.doi.org/10.1111/j.1365-2958.2006.05373.x>.
 75. Spikes S, Xu R, Nguyen CK, Chamilos G, Kontoyiannis DP, Jacobson RH, Ejzykowicz DE, Chiang LY, Filler SG, May GS. 2008. Gliotoxin production in *Aspergillus fumigatus* contributes to host-specific differences in virulence. *J Infect Dis* 197:479–486. <http://dx.doi.org/10.1086/525044>.
 76. Reeves EP, Messina CGM, Doyle S, Kavanagh K. 2004. Correlation between gliotoxin production and virulence of *Aspergillus fumigatus* in *Galleria mellonella*. *Mycopathologia* 158:73–79. <http://dx.doi.org/10.1023/B:MYCO.0000038434.55764.16>.
 77. Sugui JA, Pardo J, Chang YC, Zarembek KA, Nardone G, Galvez EM, Müllbacher A, Gallin JI, Simon MM, Kwon-Chung KJ. 2007. Gliotoxin is a virulence factor of *Aspergillus fumigatus*: gliP deletion attenuates virulence in mice immunosuppressed with hydrocortisone. *Eukaryot Cell* 6:1562–1569. <http://dx.doi.org/10.1128/EC.00141-07>.
 78. Dewitt S, Tian W, Hallett MB. 2006. Localised PtdIns(3,4,5)P₃ or PtdIns(3,4)P₂ at the phagocytic cup is required for both phagosome closure and Ca²⁺ signalling in HL60 neutrophils. *J Cell Sci* 119:443–451. <http://dx.doi.org/10.1242/jcs.02756>.
 79. Riedl J, Crevenna AH, Kessenbrock K, Yu JH, Neukirchen D, Bista M, Bradke F, Jenne D, Holak TA, Werb Z, Sixt M, Wedlich-Soldner R. 2008. Lifeact: a versatile marker to visualize F-actin. *Nat Methods* 5:605–607. <http://dx.doi.org/10.1038/nmeth.1220>.